XII International Conference on Computational Plasticity. Fundamentals and Applications
COMPLAS XII
E. Oñate, D.R.J. Owen, D. Peric and B. Suárez(Eds)

A MESOSCALE FINITE ELEMENT SIMULATION OF INTERMITTENT PLASTIC FLOW OF MICROPILLAR COMPRESSION UNDER HYBRID LOADING MODE

X. Zhang* and F. Shang†

* State Key Laboratory for Strength and Vibration of Mechanical Structures, School of Aerospace
Xi'an Jiaotong University, Xi'an 710049, P. R. China
Email: zhangxuqing@stu.xjtu.edu.cn

† Email: shangfl@mail.xjtu.edu.cn, Web page: http://gr.xjtu.edu.cn/web/shangfl

Key words: Crystal plasticity, Strain burst, Finite element simulation, Micropillar.

Abstract. The plastic deformation of the micropillar proceeds as a series of strain bursts, showing an intermittent plastic flow. In this work, we present a stochastic finite element method in crystal plasticity to describe the intermittent characteristic of crystal deformation under the hybrid loading mode (HLM). The microscopic boundary conditions(MBCs) using the HLM are studied and they are demonstrated to be different in various deformation periods such as loading stage, burst slip and holding stage, which occur alternatively as the plastic flow proceeds. In order to determine the MBCs, we use the Monte Carlo (MC) stochastic model to predict the amplitude of the burst displacement and then incorporate such model into our established continuum framework accounting for the characteristics of the strain burst. By implementing this continuum model into the finite element analysis, we predict the plastic flow of single crystal nickel micropillars that deform under uniaxial compression along the [2 6 9] crystalline direction. The simulation results indicate clearly visible strain bursts in the course of plastic deformation, producing a stair-case like stress-strain behavior that agrees well with experimental observations. The computational results reveal that the intermittent flow in the micrometer-scale is intensified due to the increasing amplitude of the strain burst, as well as the occurrence of successive strain bursts rather than the discrete strain bursts, with decreasing of the specimen size. In addition, the micropillar displacement in the context of burst activity predicted from our simulations is similar to the experimental observations. We demonstrate that our simulation method could provide further insights into the intermittent plastic flow characteristics such as burst time duration, micropillar velocity; plus, it is feasible to apply this method to investigate the plastic flow behaviors under complex loading conditions.

1 INTRODUCTION

The intermittent characteristic of crystal deformation is suggested to be an intrinsic feature in plasticity [1]. This feature is characterized by a series of burst events as revealed by many compression tests of single crystal micropillars [2]. Althrough crystal plasticity theory [3] is selectively useful for describing crystalline deformation as a basic framework, such theory fails to account for the intermittent deformation phenomenon in micropillar plasticity. In

addition, some powerful simulation techniques such as three-dimensional (3-D) dislocation dynamics (DD) simulations are still today a formidable challenge for mesoscale plasticity [4].

Alternatively, attempts have been made to directly correlate the proper constitutive model to the finite element (FE) analysis. Although the strain burst occurs in the form of dislocation instabilities and arise from the collective, avalanche-like motion of the dislocations, they are not necessarily or may not always give rise to macroscopic deformation instabilities. For samples of larger sizes, the reported experimental stress-strain curves are relatively smooth, especially for the intermittent deformation arising from the destruction of jammed dislocation configurations. This suggests the applicability of continuum models [5] and the corresponding boundary-value problems are still well-posed and contribute to the uniqueness, convergence of the solutions in FE calculations. In most cases, the FE simulations have been used with the classic crystal plasticity models because they can analyze microscopic heterogeneity associated with plastic deformation in materials. But for mesoscale plasticity, the traditional crystal plasticity models cannot represent intermittent characteristic of crystal deformation due to the lack of consideration of complex interplay of experimental loading mode, material behavior and specimen size during the plastic process. It is the objective of this work to conduct FE simulations based on a new continum model to describe the intermittent characteristic of crystal deformation.

2 MATERIAL MODEL

2.1 Stochastic microscopic boundary conditions

Figure 1 shows the plot of the actual displacement versus time curve from the micro-compression test driven by HLM [6]. The burst slip is described by the curve portion with positive slope, suggesting a higher velocity than that preprogrammed by the nanoindentation system. Then it is followed by a horizontal line or a line with small positive slope, indicating a holding stage which lasts until the actual micropillar displacement (which is linear with time) reaches the applied loading displacement by the nanoindentation system. After that, a loading stage may occur with the constant strain rate loading process. On the basis of these observations, the typical plastic flow expressed in the stress-strain curve normally includes three distinct parts: loading stage, burst slip part, and the holding stage. The corresponding boundary conditions imposed on the top surface of the micropillar are described below and they are represented by the superscripts l, b and h, respectively.

Loading stage:

$$v = L \cdot \dot{\varepsilon}_0, \quad \text{on top surface} \tag{1}$$

where v is the velocity of the top surface of the micropillar, and L is the length of the micropillar.

Burst slip period:

$$f = 0,\ u = L \cdot \delta E, \quad \text{on top surface} \tag{2}$$

where f and u are the traction and displacement on the micropillar top surface, respectively. Here, δE could be predicted using a Monte Carlo (MC) stochastic method, and then the displacement boundary value u is determined accordingly.

Holding stage:

$$f = 0\,,\ u = 0\,,\quad \text{on top surface} \tag{3}$$

In the following section, we will develop a continuum model accounting for the boundary conditions as described above.

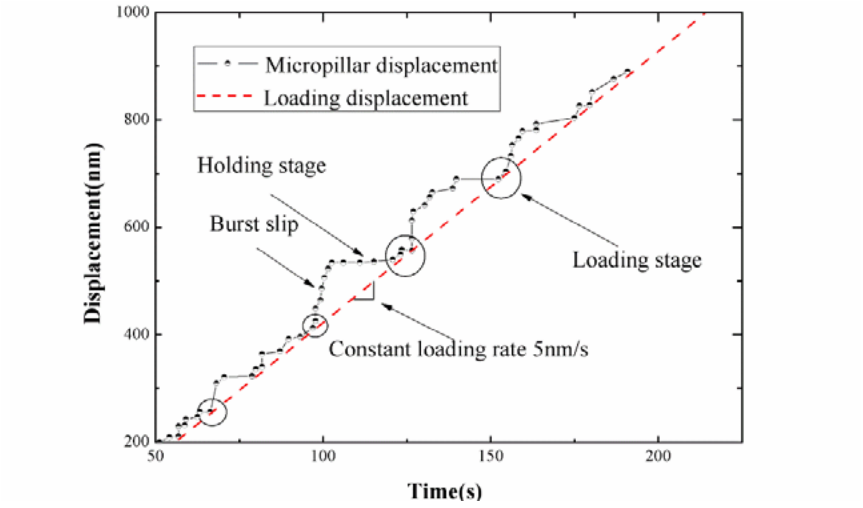

Figure 1: True experimental displacement versus time curve taken from the micro-compression test of ~20μm diameter driven by HLM

2.2 Foundation of crystal plasticity

The kinematics of FCC crystals described below is well-established and the detailed formulations are given, for example, in [7]. The total deformation gradient tensor $\mathbf{F}$ can be decomposed into the elastic tensor $\mathbf{F}_e$, and the plastic tensor $\mathbf{F}_p$:

$$\mathbf{F} = \mathbf{F}_e\mathbf{F}_p \tag{4}$$

where $\mathbf{F}_e$ represents the rotation and stretching of the lattice, $\mathbf{F}_p$ represents the plastic shear of the materials that does not change the lattice orientation and spacing. The plastic part of velocity gradient L_p is defined as:

$$\mathbf{L}_p = \mathbf{F}_e \cdot \dot{\mathbf{F}}_p \cdot \mathbf{F}_p^{-1} \cdot \mathbf{F}_e^{-1} = \sum_{\alpha=1}^{n} \dot{\gamma}_\alpha \mathbf{s}_\alpha^* \otimes \mathbf{n}_\alpha^* \tag{5}$$

in which the shear rate $\dot{\gamma}_\alpha$ on the αth slip system, is derived using a visco-plastic power-law expression as

$$\dot{\gamma}_\alpha = \dot{\gamma}_0 \operatorname{sgn}\left(\frac{\tau_{(\alpha)}}{g_{(\alpha)}}\right)\left(\frac{\tau_{(\alpha)}}{g_{(\alpha)}}\right)^m,\ \tau_{(\alpha)} = \mathbf{P}_\alpha : \boldsymbol{\sigma},\ \dot{g}_{(\alpha)} = \sum_{\alpha=1}^{n} h_{\alpha\beta}\left|\dot{\gamma}_\beta\right| \tag{6}$$

where m is the rate sensitivity exponent, $\dot{\gamma}_0$ is the shear rate at a reference condition. $\tau_{(\alpha)}$ is the resolved shear stress, which is induced by the Cauchy stress $\boldsymbol{\sigma}$ .The value $g_{(\alpha)}$ characterizes the current strain hardening state of the αth slip system. The hardening matrix $h_{\alpha\beta}$ takes the form [3]:

$$h_{\alpha\beta} = q h_{\alpha\alpha},\ h_{\alpha\alpha} = h_0 \operatorname{sech}^2\left|\frac{h_0\gamma}{\tau_s - \tau_0}\right|,\ \gamma = \sum_{\alpha=1}^{n}\int_0^t \left|\dot{\gamma}_\alpha\right| dt \tag{7}$$

where q describes the latent hardening behavior, and which is assumed to be 1.0 for coplanar and 1.4 for non-coplanar slip systems. h_0 is the initial hardening modulus, τ_0 is the initial value of the critical resolved shear stress (CRSS) and τ_s is the shear stress saturated at stage I.

The constitutive equation is specified by

$$\hat{\boldsymbol{\sigma}} = \boldsymbol{\Lambda} : \dot{\boldsymbol{\varepsilon}} - \sum_{\alpha=1}^{n} \boldsymbol{\Gamma}_\alpha \dot{\gamma}_\alpha \tag{8}$$

in which $\hat{\boldsymbol{\sigma}}$ is the Jaumann stress rate, $\boldsymbol{\Gamma}_\alpha = \mathbf{C} : \mathbf{p}_\alpha + \mathbf{w}_\alpha \cdot \boldsymbol{\sigma} - \boldsymbol{\sigma} \cdot \mathbf{w}_\alpha$ and $\Lambda_{ijmn} = \mathrm{C}_{ijmn} - \sigma_{ij}\delta_{mn}$. Here, $\mathbf{C}$ is the tensor of the elastic modulus. A more detailed description of the crystal plasticity constitutive model can be found in [3,7].

2.3 Accounting for strain burst

We account for the strain burst in the continuum model from two aspects. We first seperate the burst slip from the loading stage by considering a small dimensionless constant, and then judge its occurrence through the load serrations. The validation of the strain burst will be described in section 3.3.

Figure 2 shows the typical schematic diagram of the history of strain rate in the loading stage, burst slip and holding stage. The burst slip occurs with a jump of strain rate $\dot{\gamma}_\alpha^b(t^+)$ from the $\dot{\gamma}_\alpha^l(t^-)$ evolving in the loading stage that begins at time t-Δt^l with a strain rate of $\dot{\gamma}_\alpha(t-\Delta t^l)$. Such event ends up with a strain rate of $\dot{\gamma}_\alpha(t+\Delta t^b)$ truncated by the $\dot{\gamma}_{\mathrm{th}}$ as an definition of active time step Δt^b. After that, the holding stage occurs associated with no shear rate in an idealized situation. It should be mentioned that the $\dot{\gamma}_\alpha(t+\Delta t^b+\Delta t^h)$ can represent either the beginning of the loading stage or the burst slip as suggested later.

As seen in figure 2, the expression of $\Delta\gamma^l$ could be written as:

$$\Delta\gamma^l = \dot{\bar{\gamma}}_\alpha^l(\xi)\cdot\Delta t^l = \left[(1-\xi)\dot{\gamma}_\alpha(t-\Delta t^l) + \xi\dot{\gamma}_\alpha(t^+)\right]\Delta t^l \tag{9}$$

by adjusting the value of $\xi \in (0,1)$. The burst slip is studied by combining with the holding stage, and then we obtain the shear strain increment $\Delta\gamma^b$ by

$$\Delta\gamma^b = \dot{\bar{\gamma}}_\alpha^b(\xi)\cdot\Delta t^b = \left[(1-\xi)\dot{\gamma}_\alpha(t^+) + \xi\dot{\gamma}_\alpha(t+\Delta t^b+\Delta t^h)\right]\Delta t^b \tag{10}$$

Here, ξ is determined from the loading stage. Normally, the burst activity is characterized by a higher strain rate and larger strain increment $\Delta\gamma^b$ when compared with the loading stage. On the one hand, when the burst displacement is large enough, $\dot{\gamma}_\alpha(t+\Delta t^b+\Delta t^h)$ possibly represents an initial jump rate of the burst slip (the variables at initial time t are known), suggesting a succession of additional displacement events, as frequently observed in many tests. On the other hand, if $\Delta\gamma^b$ is featured with a moderate bust size, $\dot{\gamma}_\alpha(t+\Delta t^b+\Delta t^h)$ possibly represents a negligible strain rate of the loading stage due to the viscous deformation as assumed in the loading stage. This is the case since the stain bursts are frequently observed to be separated by the loading stage in micro-compression tests. Thus, the value ξ derived from the loading stage, could be also applied to the strain burst process consisting of burst slip and holding stage.

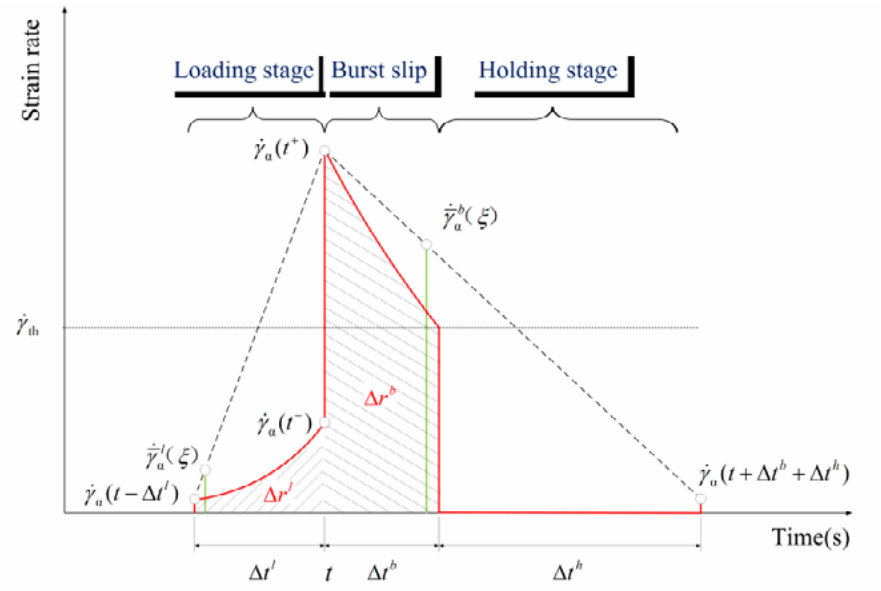

Figure 2: Schematic description of the history of strain rate in the loading stage, burst slip and holding stage (red lines). Green lines represent the average strain rate $\dot{\bar{\gamma}}_\alpha$ that is computed by Δr (shadow area).

For simplicity, we assume that ξ is a dimensionless constant. Considering equations (9) and (10), the average shear increment rate $\dot{\bar{\gamma}}_\alpha$ can be written as a general form:

$$\dot{\bar{\gamma}}_\alpha(\xi) = (1-\xi)\dot{\gamma}_\alpha(t) + \xi\dot{\gamma}_\alpha(t+\Delta t^+) \tag{11}$$

Here, a smaller value of ξ could lead to a faster strain rate in the burst slip compared to that of the loading stage, and thus separates the two processes. Additionally, when the two processes evolve, the produced strain rate fluctuations can render the load serrations due to the constant strain rate programmed by the nanoindentation system.

2.4 Burst slip judgment

Since the loading stage sustains an increasing load as described in section 2.1, the produced engineering stress S_1 satisfies:

$$\dot{S}_1 \cdot S_1(t) > 0 \tag{12}$$

On the contrary, an occurrence of burst slip satisfies:

$$\dot{S}_1 \cdot S_1(t) \le 0 \tag{13}$$

where $\dot{S}_1$ could be related with the rate of stress by $\dot{S}_1 = \langle \dot{\sigma}_1 \rangle = \frac{1}{V}\int_V \dot{\sigma}_1 \mathrm{d}V$, V is the current volume of the sample.

In summary, we could propose a constitutive model that describes the plastic flow in the form of a piecewise function as follows:

$$\Delta\boldsymbol{\sigma} = \begin{cases} \boldsymbol{\Lambda} : \Delta\boldsymbol{\varepsilon}(\Delta t) - \sum_{\alpha=1}^{n} \boldsymbol{\Gamma}_\alpha \Delta\overline{\gamma}_\alpha(\Delta t); & \dot{S}_1 \cdot S_1(t) > 0 \quad \text{(a)} \\ \boldsymbol{\Lambda} : \Delta\boldsymbol{\varepsilon}(\Delta t) - \sum_{\alpha=1}^{n} \boldsymbol{\Gamma}_\alpha \Delta\overline{\gamma}_\alpha(\Delta t^b); & \dot{S}_1 \cdot S_1(t) \le 0 \quad \text{(b)} \end{cases} \tag{14}$$

Noted that expression (14b) is obtained by fixing the value of time increment $\Delta t = \Delta t^b + \Delta t^h$. Such time increment is related with the amplitude of the strain burst by $\Delta t = \delta E / \dot{\varepsilon}_0$, wherein the magnitude of δE should be in the range between its lower limit $\delta E_{\min}$ and upper limit $\delta E_{\max}$, as discussed in [8].

3 FINITE ELEMENT SIMULATION

3.1 Simulation setup

The geometric details of the model used in the analysis are presented in Figure 3. This configuration is roughly equivalent to that of the actual micro-compression testing samples [9]. The boundary conditions used in our simulation mimic the experimental conditions with the displacements prescribed along the *y*-direction and the bottom of substrate is fixed. In addition, the loading axis is chosen to align along the [2 6 9] single-slip direction. To imitate the loading conditions of the real experiments, the loading velocity is set as the constant displacement rate of 1.0×10^{-4}/s for all the simulations. C3D8 type elements with full integration are used to discretize the model. The following parameters are used for both

samples: elastic modulus $c_{11}=246.5\text{GPa}$, $c_{12}=147.3\text{GPa}$, $c_{44}=124.7\text{GPa}$; $\dot{\gamma}_0=0.001$, $q=1.4$. And, for bulk cyrstal: $\tau_0=19\text{MPa}$, $\tau_s=40\text{MPa}$, $h_0=32\text{MPa}$, $m=0.0005$, $\delta E_{\min}=1.4\times10^{-7}$, $\delta E_{\max}=2.2\times10^{-5}$; for micropillar: $\tau_0=40\text{MPa}$, $\tau_s=46\text{MPa}$, $h_0=85\text{MPa}$, $m=0.01$, $\delta E_{\min}=4.3\times10^{-5}$, $\delta E_{\max}=7.8\times10^{-3}$.

3.2 Stress-strain behavior

Figure 3 compares the calculated shear stress versus shear strain curves for Ni micropillars having diameter ~10μm and bulk crystal, with those from the experimental tests [9]. For each specimen size, the corresponding parameters, as given above, are chosen by fitting the experimental stress-strain curve (see figure 3). It is shown that the predicted stress-strain behaviors are nearly comparable with experimental observations at both macroscopic and microscopic levels. For the microsamples of ~10μm, the stair-case like steps are clearly visible on the stress-strain curves, associated with constant stresses. These steps always consist of series of smaller steps occurring in succession, which are separated by the loading stages, thus giving rise to the intermittent flow. For the bulk crystal, despite the observed smooth stress-strain curve, the steps are still successfully captured in the simulations and they actually were observed. In addition, we could also see that, with the decreasing specimen size, the overall shape of the simulated flow curves exhibit severely intermittent flow that are characterized by much larger steps. And this is consistent with the actual experimental observation.

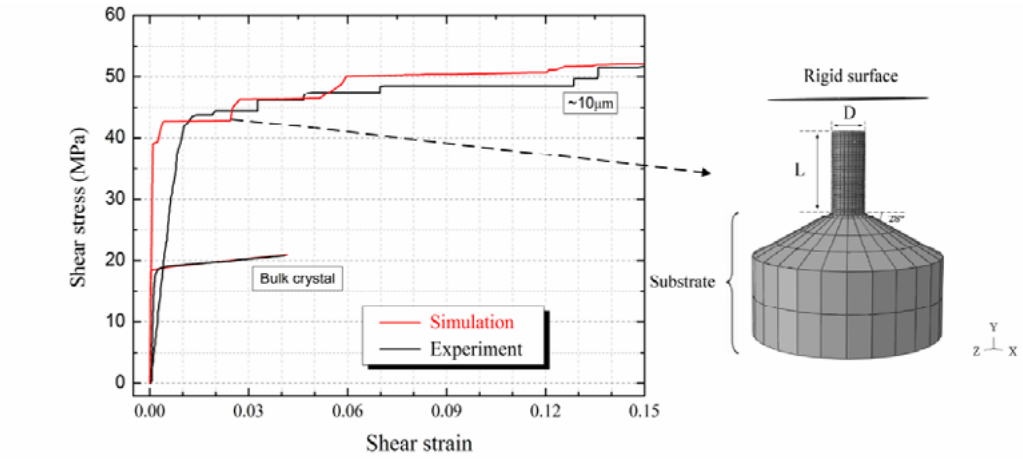

Figure 3: Left: comparison of the shear stress versus strain responses between simulations and experiments: micro-compression tests of [2 6 9] nickel pillars with diameters of ~10μm and bulk crystal, respectively; Right: finite element model for the micropillar. *D* and *L* represent the pillar diameter and length, respectively.

3.3 Verification of strain burst

In this section, we verify the stair-case like steps to be strain bursts. Normally, a burst activity is featured with (i) high strain rate; and (ii) its occurence in the form of instability.

To illustrate the higher strain rate of the strain burst, we plot the average strain rate of micropillar and the shear stress as a function of time for ~10μm diameter in figure 4. It is seen that as the plastic deformation proceeds, many step-case-like sections emerge, suggesting a deviation from the programmed displacement (presented by the dash line in red) where the displacement rate is ~2.2nm/s, corresponding to the constant strain rate of 1.0×10^{-4}/s. In these sections, the micropillar displacements all exceed the programmed displacement, thus suggesting the higher average strain rate. When the former coincides with the latter, a loading stage occurs. Our results reveal that the displacements increase mainly in the form of discrete step-case-like sections. Although there are some sections like loading stages, we found that they actually include many tiny strain bursts, much similar to the response of the bulk crystal. In addition, we also see that the sizes of step-case-like sections vary widely, as the stochastic nature of the strain burst is considered in the proposed model. These behaviors are quite consistent with the actual compression testing results of pure Ni, which was also obtained under the HLM [9]. In practice, those higher strain rates events are commonly identified as strain bursts in the micropillar tests.

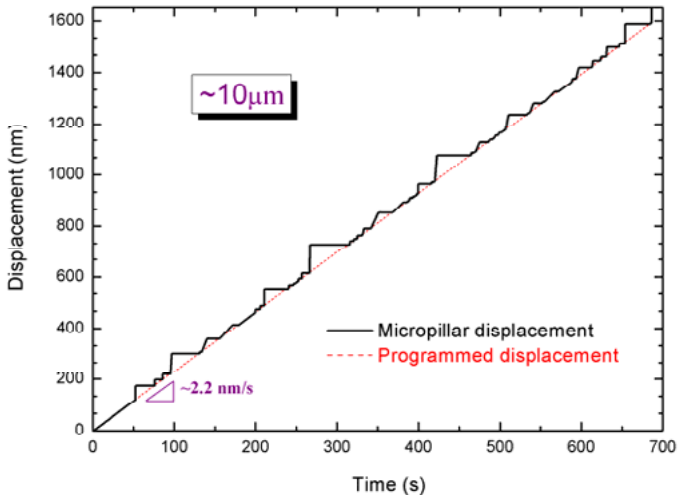

Figure 4: Predicted displacement versus time curve from the micro-compression test of ~10μm diameter Ni micropillar

Plastic instabilities often reflect at the macroscopic stress-strain response as strain bursts. For bulk crystals, such instabilities are necessarily associated with localization of deformations, such as intense shear bands and discrete slip lines. For microsamples, the experimentally observed strain bursts are also suggested to be associated with discrete slip lines [10]. In other words, the strain bursts occur in the form of instabilities during the plastic flow of microsamples. These instabilities could be illustrated using a widely used energy-based stability criterion as proposed in [11], and it is expressed mathematically as the second-order work involving both incremental stress and strain fields. This criterion plays an important role to envisage the onset of instabilities, and has been employed to capture the strain burst phenomenon in the necking of a metal sheet [12].

As suggested in [11], the sufficient condition of stability described by the second-order work criterion per unit volume of material is given by

$$d^2w_2 = \Delta\boldsymbol{\sigma}\left(\Delta t\right) : \Delta\boldsymbol{\varepsilon}\left(\Delta t\right) > 0 \quad \forall\Delta\boldsymbol{\varepsilon}\left(\Delta t\right) \neq \mathbf{0} \tag{15}$$

Here, d^2w_2 is the second-order work, which is analyzed at the material point in the body. The negative values or vanish of the second-order work, expressed in equation (15), may lead to the local instability. If local instabilities are pervasive within the crystalline solids, the globe instability possibly occurs, and the global second-order work d^2W_2 can be computed from

$$d^2W_2 = \int_V \Delta\boldsymbol{\sigma}(\Delta t) : \Delta\boldsymbol{\varepsilon}(\Delta t)\, dV \tag{16}$$

Figure 5 shows an example of the evolution of the global second-order work d^2W_2 and shear stress as a function of time for ~10μm diameter Ni micropillar. It is seen that the appearance of stair-case like events correspond to the small and negative values of d^2W_2, in contrast to the loading stage, which leads to the positive values of d^2W_2. This suggests that the stair-case like event occurs in the form of instability.

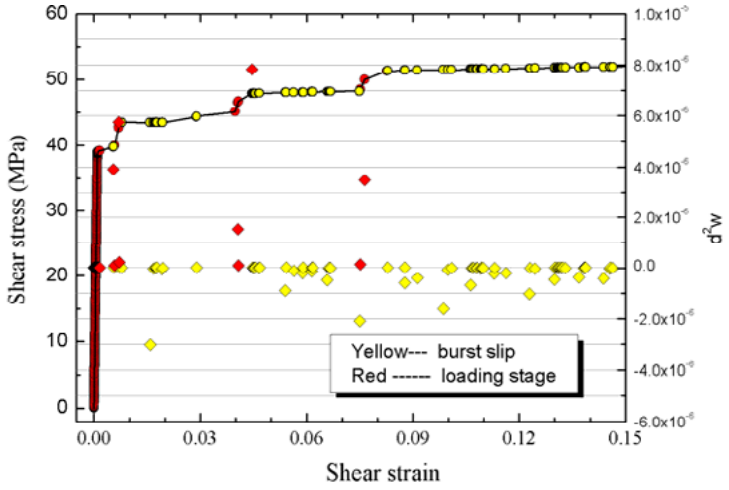

Figure 5: The evolution of the second-order work (diamond) and shear stress (circular) as fuction of the shear strain for the microsample of ~10μm diameter

4 DISCUSSION

The proposed continuum model has focused mainly on the intermittent deformation behavior of micropillar samples having a single-slip orientation. The required material parameters in such model can be classified into four parts: (i) strain burst parameters ($\delta E_{\min}$, $\delta E_{\max}$); (ii) PAN hardening model parameters (τ_0, τ_s, h_0). (iii) elastic modulus constants (c_{11}, c_{12}, c_{44}); (iv) flow rule parameters ($\dot{\gamma}_0$, m). Compared with the classic crystal plastic finite element method (CPFEM), only the material parameters in Part (i) are

introduced additionally and they are employed to account for the size-dependent strain burst phenomenon. For the parameters in the rest parts (ii~iv), the strategies of determining them show no difference between our model and the CPFEM method.

Our simulation results could capture the most essential aspects of the intermittent deformation observed in the compression tests of the single crystal micropillars. As seen in figure 3, the macroscopic stress-strain curve for the bulk crystal, are in good agreement with that of experiments. However, our model could identify a series of strain bursts during the simulated plastic flow process. Additionally, as the specimen size decreases, the intensified plastic flow could also be well represented based on the new proposed continuum model. These results are suggestive of the universality of the strain burst behavior in plasticity. Figure 5 shows few loading stages occured during the plastic flow, suggesting that the intermittet flow proceed through a series of strain bursts. Based on these observations, we could conclude that the remarkable intermittent flow in micro-scale is attributed to both the increasing probability of the occurrence of successive strain bursts and the increasing amplitude of the strain burst, with decreasing specimen size. Furthermore, figure 5 also reveals that the second-order work criterion has excellent capability of capturing the emergency of the strain burst during the plastic flow. We shall mention that, although the load serration could be applied to judge the strain burst for the uniaxial deformation as commonly used in the 3D-DDS, its application may not suitable to the complex boundary problems such as microbending, 3D shear deformation. Thus, the use of the second-order work criterion seems to have certain advantage over the loading serration criterion, as a strain burst criterion.

Finally, it is worth mentioning that, although only the micropillar displacement in context of burst activity is studied here, the finite element analysis based on the proposed model could be used to investigate the issues such as the burst duration, strain rate and strain rate sentivity as well. These computational efforts are underway. It is believed that such investigations will provide useful insights for the understanding of other burst characteristics such as the burst time duration, and other mechanical mechanisms.

5 CONCLUSIONS

- Our simulations clearly show visible strain bursts during the plastic flow, and the predicted behavior of the stress-strain response is qualitatively comparable with the experimental observations.
- For the bulk crystal, we could identify a series of strain bursts during the simulated plastic flow process, which is suggestive of the universality of the strain burst behavior in plasticity.
- The simulation results of the micropillars demonstrated that many strain bursts occur in a successive way.
- The second-order work criterion has excellent capacity of capturing the emergency of the strain burst during the plastic flow.

REFERENCES.

[1] Csikor, F.F., Motz, C., Weygand, D., Zaiser, M. and Zapperi, S. Dislocation avalanches,

Strain bursts, and the problem of plastic forming at the micrometer scale. *Science* (2007) **318**: 251-254.

[2] Uchic M.D, Dimiduk D.M, Florando J.N. and Nix W.D. Sample dimensions influence strength and crystal plasticity. *Science* (2004) **305**: 986–89.

[3] Asaro, R.J. and Needleman, A. Texture development and strain hardening in rate dependent polycrystals. *Acta Metall* (1985) **33**: 923–953.

[4] Dimiduk, D.M., Nadgorny, E.M., Woodward, C., Uchic, M.D. and Shade, P.A. An experimental investigation of intermittent flow and strain burstscaling behavior in LiF crystals during microcompression testing. *Philosophical Magazine* (2010) **90**: 3621-3649.

[5] Hurtado, D.E. and Ortiz, M. Surface effects and the size-dependent hardening and strengthening of nickel micropillars. *Journal of the Mechanics and Physics of Solids* (2012) **60**: 1432-1446.

[6] Dimiduk, D.M., Woodward, C., LeSar, R. and Uchic, M.D. Scale-free intermittent flow in crystal plasticity. *Science* (2006) **312**:1188-1190.

[7] Asaro, R. and Lubarda, V. *Mechanics of Solids and Materials* (2006). Cambridge University Press.

[8] Zhang, X., Pan, B. and Shang, F. Scale-free behavior of displacement bursts: Lower limit and scaling exponent. *Europhysics Letters* (2012) **100**: 16005.

[9] Dimiduk, D.M, Uchic, M.D. and Parthasarathy, T.A. Size-affected single-slip behavior of pure nickel microcrystals. *Acta Mater* (2005) **53**: 4065–4077.

[10] Schwerdtfeger, J., Nadgorny, E., Koutsos, V., Blackford, J.R. and Zaiser, M. Statistical heterogeneity of plastic deformation: An investigation based on surface profilometry. *Acta Materialia* (2010) **58**: 4859-4870.

[11] Hill, R. A general theory of uniqueness and stability in elastic–plastic solids. *J. Mech. Phys.Solids* (1958) **6**: 239–249.

[12] Bassani, J. L. and Racherla, V. From non-planar dislocation cores to non-associated plasticity and strain bursts. *Progress in Materials Science* (2011) **56**: 852-863.